Earth Reinforcement, Ochiai, Yasufuku & Omine (eds) © 1997 Balkema, Rotterdam, ISBN 9054108339

Discussion leader's report: Embankments

D.T. Bergado & P.V. Long
School of Civil Engineering, Asian Institute of Technology, Bangkok, Thailand

1 INTRODUCTION

In this Session 1 on Embankments, a total of 20 papers has been submitted. The papers can be roughly classified into 4 groups as follows:

1) Design and analyses (7 papers)
2) Modeling and full scale tests (7 papers)
3) Reinforced soil structures spanning pile foundation or voids (3 papers)
4) Dynamic response of geosynthetic reinforced structures (3 papers)

2 DESIGN AND ANALYSES

In this category, the papers of the following authors are included, namely: Ochiai et al, Kaniraj, Arai and Kasahara, Acevedo and Martinez, Yang et al, Yeo et al, and Wong. For geotextile reinforced embankment on soft ground, three issues are involved, namely: (a) Inclination of the reinforcing force, (b) Mobilized strains in the geotextile reinforcement, (c) Modification of shear strength at the failure plane, and (d) Effect of confinement on the properties of the geotextile reinforcement. Accordingly the research directions are mostly directed into these issues. The first three issues have been addressed by the submitted papers and further elaborated herein.

The effect of reinforcement on soil strength at the failure plane has been presented by Long et al (1996) and illustrated in Fig. 1. The tensile force mobilized in the reinforcement, T_{mob}, can be decomposed into 2 components:

$$Tangential: \quad T_p = T_{mob}(\cos\beta) \qquad (1)$$

$$Normal: \quad T_n = T_{mob}(\sin\beta) \qquad (2)$$

The projection of the resistant force on the tangent direction is given as follows:

$$T_r = T_p + T_n(\tan\phi) = T_{mob}(\cos\beta + \sin\beta\tan\phi) \qquad (3)$$

The resisting moment caused by the reinforcement is given as:

$$M_{rr} = T_r\,(R) \qquad (4)$$

The geotextile reinforce embankment can be assumed to be equivalent to an unreinforced embankment with the following modified parameters:

$$\phi_G = \phi \qquad (5)$$

$$C_G = C + \Delta C_G \qquad (6)$$

Then, the following expression can be written:

$$M_{rr} = \Delta C_G(\overline{AB})R \qquad (7)$$

where AB is the arc length in Fig. 1.

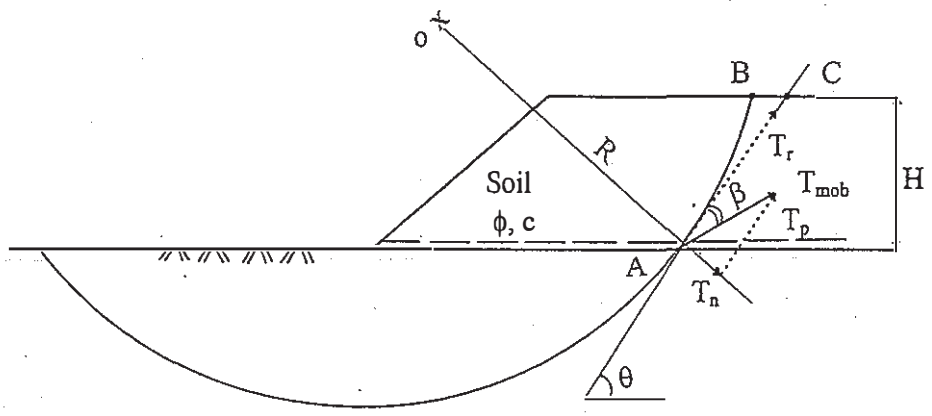

Fig. 1 Effect of Geotextile Reinforcement on Soil Strength.

Equating Equas. 4 and 7 yields:

$$\Delta C_G = \left(\frac{T_r}{\overline{AB}}\right) \tag{8}$$

Approximating the arc length AB by the straight line AC and substituting to Equa. 8:

$$\Delta C_G = \left(\frac{T_r(\sin\theta)}{H}\right) \tag{9}$$

From Equas. 3 and 9, the following expression can be obtained:

$$\Delta C_G = \left(\frac{(\alpha)T_{mob}}{H}\right) \tag{10}$$

where:

$$\alpha = (\cos\beta + \sin\beta\tan\phi)\sin\theta \tag{11}$$

The orientation and magnitude of geotextile reinforcement force with the slip failure are also the key parameters affecting on the stability analyses of reinforced embankments on soft ground. Presently, these parameters have been selected arbitrarily and even independently. Bergado et al (1996) presented the deformation behavior of geotextile reinforcement at the vicinity of the shear surface which addressed these parameters. Both the large direct shear tests with inclined geotextile reinforcements as well as as the finite element modeling for reinforced soil mass that simulate the actual conditions of slip failure in the field have been conducted.

The mobilized strain in geotextile reinforcement near the shear surface can be calculated from the displacement of the reinforcement measured at locations G_1 and G_2 in Fig. 2.

$$\varepsilon = \left(\frac{d_1 - d_2}{l_{12}}\right) \tag{12}$$

where d_1, d_2 are the measured displacements of the geotextile at points G_1 and G_2, respectively, and l_{12} is the original distance between these points. The value of l_{12} of 50 mm was set for all tests. The inclination factor, I_f, of geotextile reinforcement is expressed by the following equation:

$$I_f = 1 - \alpha/\alpha_0 \tag{13}$$

where α_0 and α, respectively, are the original and current inclination angles of the geotextiles as seen in Fig. 3. As shown in Fig. 3, for shear displacement, u, the interface surface between geotextile and backfill soil OBA moved to O'B'A'. Assuming that the current interface surface O'B'A' can be approximated by a parabola, the following expressions can be obtained: (Bergado et al, 1996):

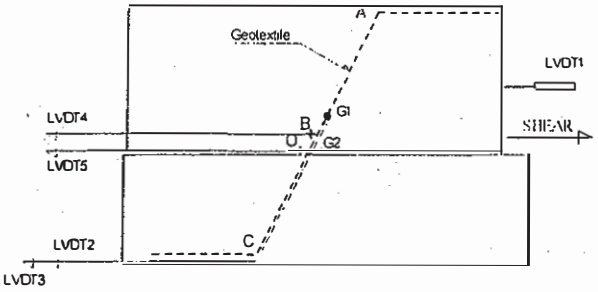

Fig. 2. Instrumentation for Large Direct Shear Test

$$\tan \alpha = \frac{Y_A X_{B'}^2 - Y_B X_{A'}^2}{X_A X_{B'}^2 - X_{B'} X_{A'}^2} \qquad (14)$$

where Y_A and Y_B are the vertical coordinates of point A and B as illustrated in Fig. 3.

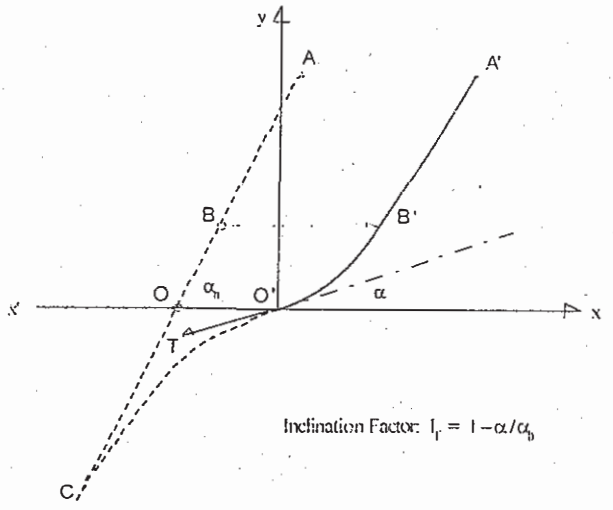

Fig. 3. Schematic diagram for calculating the inclination factor.

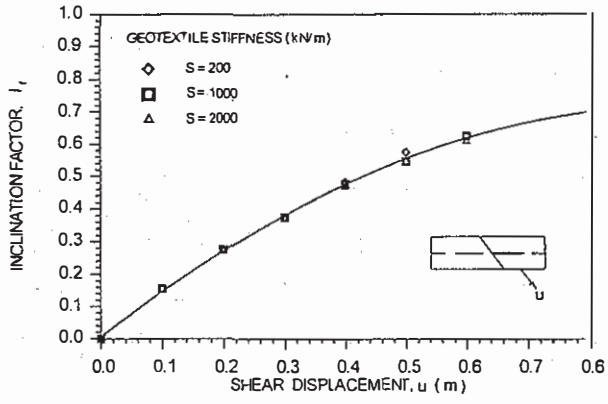

Fig. 4. Inclination factor-shear displacement plots from FEM.

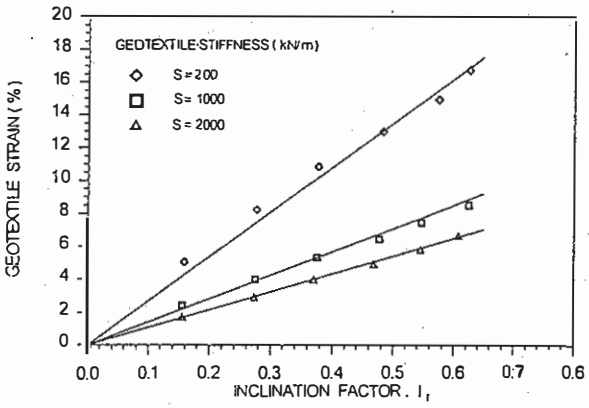

Fig. 5. Localized strain-Inclination factor plots from FEM.

The PLAXIS finite element program (Vermeer and Brinkgreve, 1995) was employed in the validation of the direct shear test results across geotextile reinforcement by conducting the back-analyses of the test data. The good agreement between the calculated and measured data has been presented by Bergado et al (1996) indicating the success of utilizing the PLAXIS software. The calculated values of inclination factor, I_f, are plotted in Fig. 4. indicated that the inclination factor is dependent on the shear displacement but not on the geotextile stiffness. As shown in Fig. 4, the value of I_f is less than 1.0 even at large displacement of 0.8 m. The values of the geotextile strain near the intersection of the reinforcement and shear surface, denoted as localized strain ε_{lc}, are presented in Fig. 5 as a function of the inclination factor. Subsequently, the relationship between localized strain, ε_{lc}, and inclination factor, I_f, can be approximated by straight lines at different geotextile stiffness. The curve fitting is plotted in Fig. 6 and the following expression can be obtained:

$$\varepsilon_{lc} = 225(I_f)S^{-0.4} \qquad (15)$$

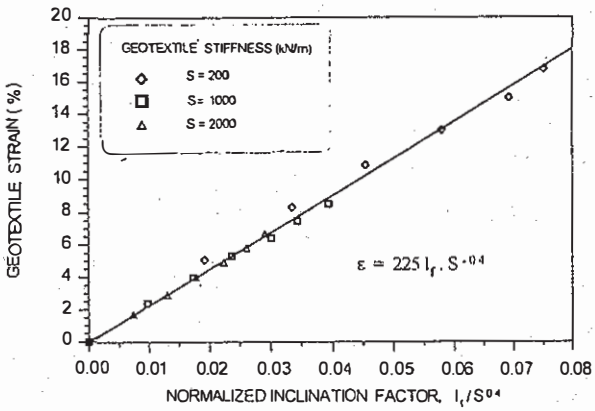

Fig. 6. Localized strain-normalized inclination factor from FEM.

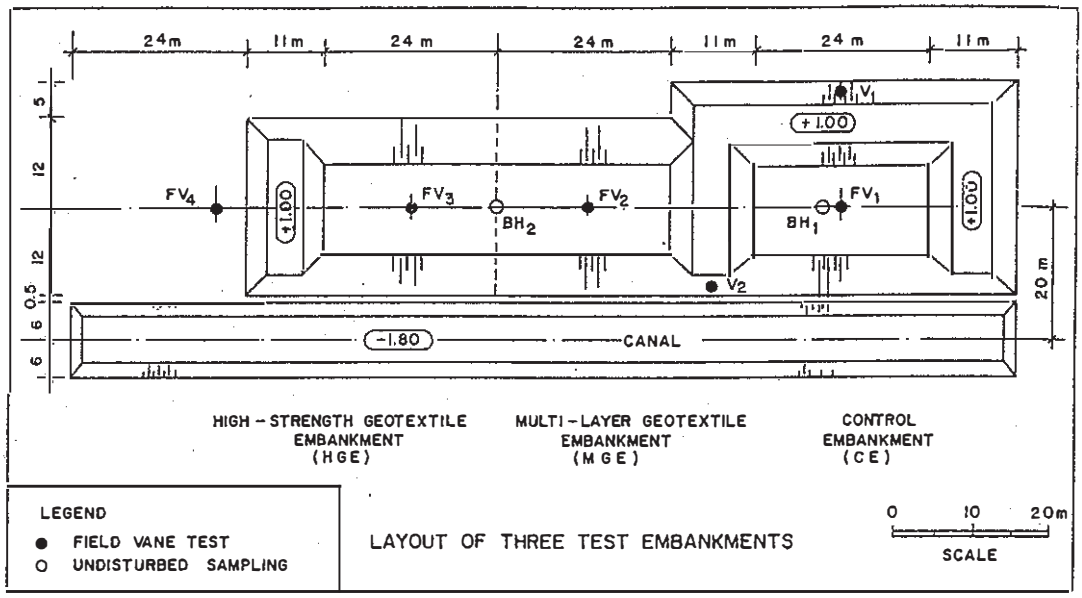

Fig. 7. Layout of the Test Embankment together with Locations of Field Investigation.

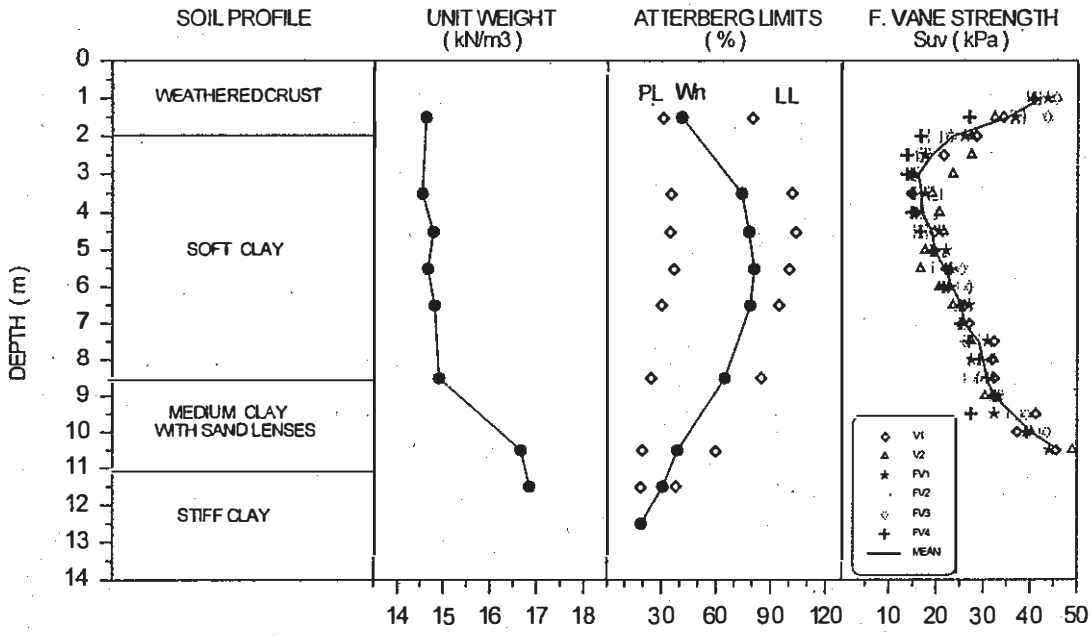

Fig. 8. General Soil Profile and Soil Properties at the Site.

Thus, the localized strain, ε_{lc}, in geotextile reinforcement associated with the slip failure has been found to be a function of geotextile stiffness and the corresponding inclination factor.

3 FULL SCALE TESTS AND MODELING

The papers in this group include those by Marolo et al, Furuya et al, Miyata et al, Sharma and Bolton, Kojima et al, Kamon et al, and Oikawa et al. The topics addressed in the submitted papers dealt with effects of reinforcement rigidity or stiffness, creep behavior of reinforcement, foundation behavior beneath reinforced structures reinforcement by geosynthetic horizontal drains (GHD), and behavior of geotextile-reinforced embankment on soft ground from centrifuge model tests and finite element modeling. The utilization of GHD reinforcement accelerated pore pressure dissipation and increased the soil shear strength for high water content cohesive embankment fills.

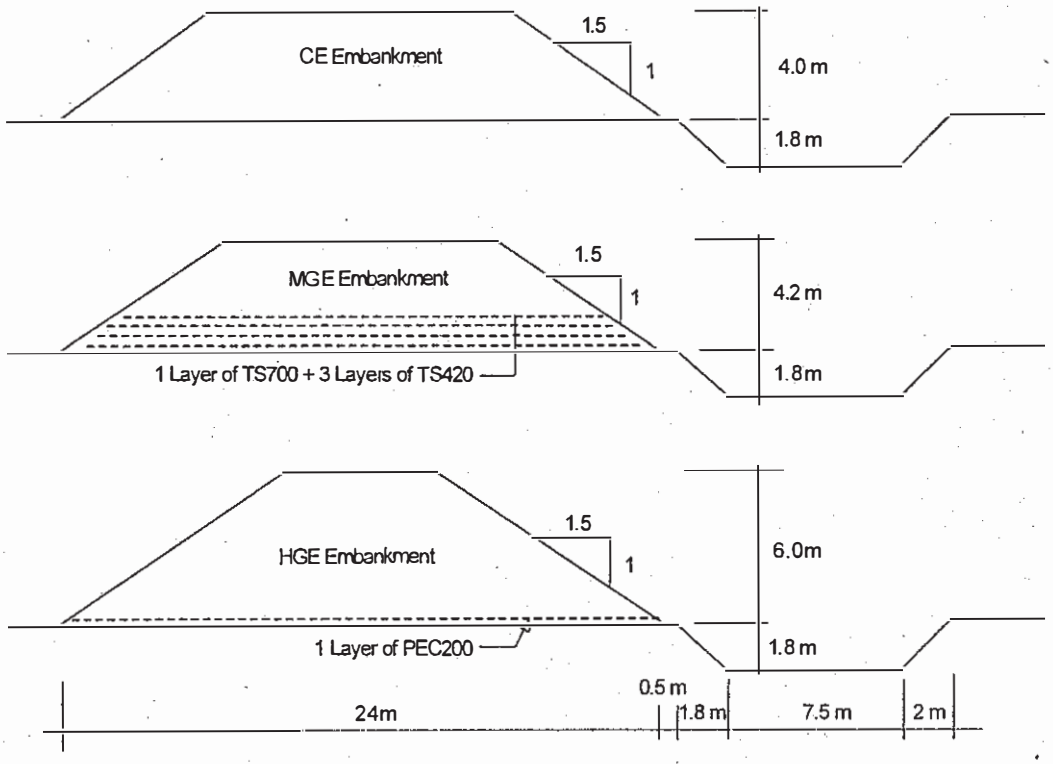

Fig. 9. Cross Sections of Three Test Embankments.

Concerning the failure mechanism and performance of geotextile reinforced embankments on soft Bangkok clay, three full scale instrumented test embankments with and without geotextile reinforcements have been constructed to failure (Bergado et al 1994a). The layout of the test embankments is shown in Fig. 7. The generalized soil profile and soil properties are presented in Fig. 8. One embankment was reinforced with multiple layers of low strength, nonwoven, needle-punched geotextile. The other was reinforced by a single layer of high strength composite woven/nonwoven geotextile. The unreinforced embankment was built nearby as a control embankment.

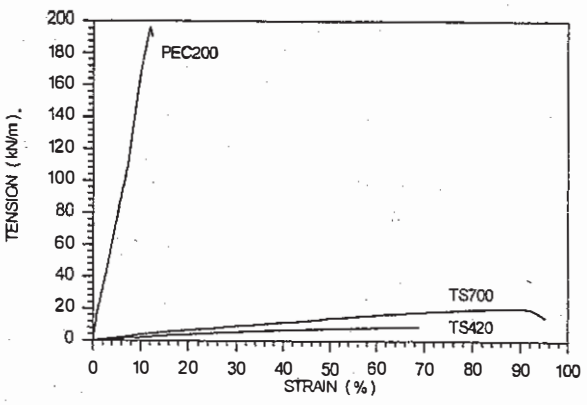

Fig. 10 In-Air Tension-Strain of Geotextile Reinforcements (ASTM D4595).

The cross-sections of the three embankments are presented in Fig. 9. All embankments were designed with 1.5 to 1.0 side slopes. A canal of 2.0 m deep and 7.5 m wide was excavated along the toe of the embankments in order to reduce the fill required for the embankment loading to failure and to ensure that the failure will occur in the proposed side. The multi-layer reinforced embankment (MGE) contained four layers of reinforcements as follows: one layer of nonwoven, needle-punched geotextile (TS-700) and three layers of nonwoven, needle-punched geotextile (TS-420). The single layer reinforced embankment (HGE) was reinforced with high strength geotextile (PEC-200) placed at the embankment base. The wide-width tensile strength versus strain relationships of the geotextile reinforcements are given in Fig. 10. The silty sand materials with maximum dry density of 18 kN/m^3 which are widely used for highway fills, was utilized as backfill materials. Standard instrumentations were installed in the foundation soils, namely: settlement plates, piezometers, and inclinometers. The displacements and strains in the geotextile reinforcements were measured by wire extensometers, Glotzl extensometers, and strain gages. Details of the foundation and geotextile

instrumentations are given by Bergado et al (1994b). The construction sequences of the three test embankments are presented in Fig. 11. Detailed description of the embankment constructions were given by Bergado et al (1994b). The embankment loading was calculated from the fill thickness and its total unit weight with adjustments due to rainfall during construction. The net embankment height is defined as the difference between the current elevation of embankment crest and the original elevation of the embankment base. In the reinforced embankment, a two step failure occurred. The primary failure corresponded to the bearing capacity failure of the foundation. The secondary failure occurred during rupture of the reinforcements. The failure of MGE embankment compared to that of the CE embankment is shown in Fig. 12.

The limit equilibrium method, assuming circular slip failure and using the PC-STABL6 software, was utilized to back-analyze the stability of the three embankments. The free body reinforcement force was utilized for the single layer reinforced (HGE) embankment. The modified soil strength was employed in the multi-layer reinforced (MGE) embankment. In this case, the resultant force in the direction tangent to the slip surface, T_r, can be calculated as in Equa. 3. The direction of the reinforcement force at onset of failure can be represented by the inclination factor, I_f, as given in Equa. 13. The limiting strain, ε_{lm}, at the onset of

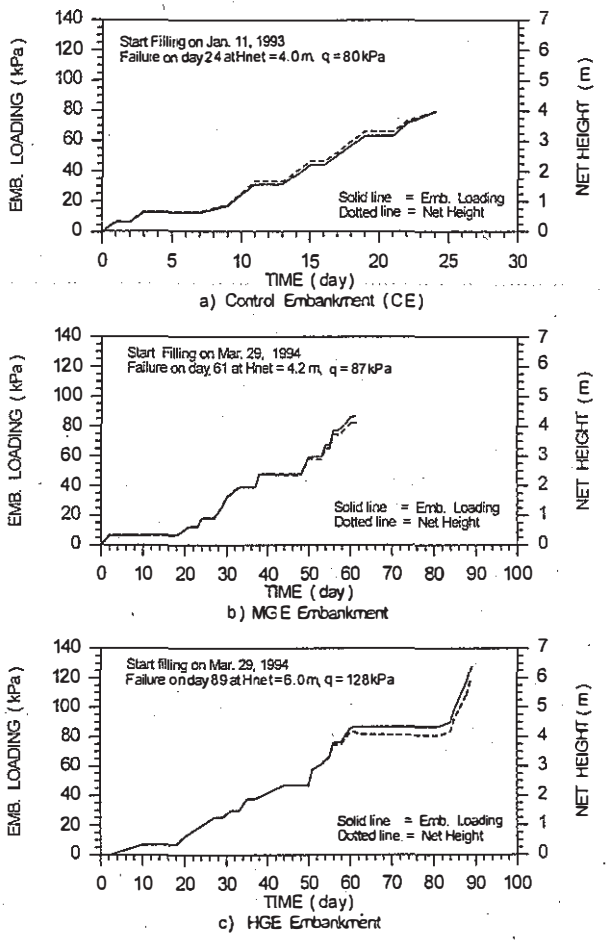

Fig. 11. Construction Sequences of Three Test Embankments.

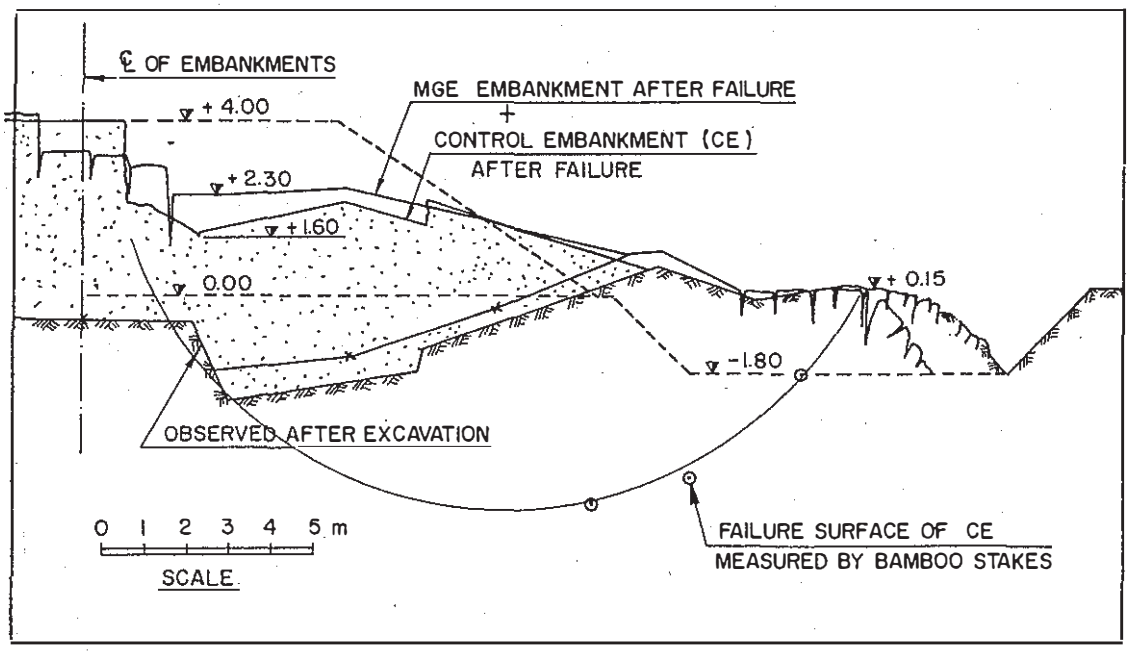

Fig. 12 Cross Section of MGE Embankment after Failure Measured on May 31, 1993.

failure can be obtained as follows:

$$\varepsilon_{lm} = \varepsilon_c + \varepsilon_{lc} \qquad (16)$$

where ε_c is the critical strain corresponding to the critical height just prior to the bearing capacity failure of foundation soil, and ε_{lc} is the localized strain associated with slip failure as given Equa. 15. The results of the back-analysis are tabulated in Table 1. The interpreted and predicted values of ε_{lc} are plotted in Fig. 13 showing good comparison for a large range of geotextile stiffness including the Sackville Embankment (Rowe et al, 1995) and Guiche Embankment (Delmas et al, 1992).

For the soft Bangkok clay, the multiple layer reinforced embankment height was 1.15 times the unreinforced embankment height using lower strength geotextile reinforcement. The single layer, high-strength geotextile reinforcement increased the embankment height to 1.5 times the unreinforced embankment height. The critical strain at primary failure can be taken as 2.5 to 3.0 %. The limiting strain at secondary failure can be taken as 12 to 14%. At primary failure the reinforcement force can be assumed in the horizontal direction,(I_f=0.0). During the secondary failure, the reinforcement force can be assumed at bisectional direction (I_f =0.50).

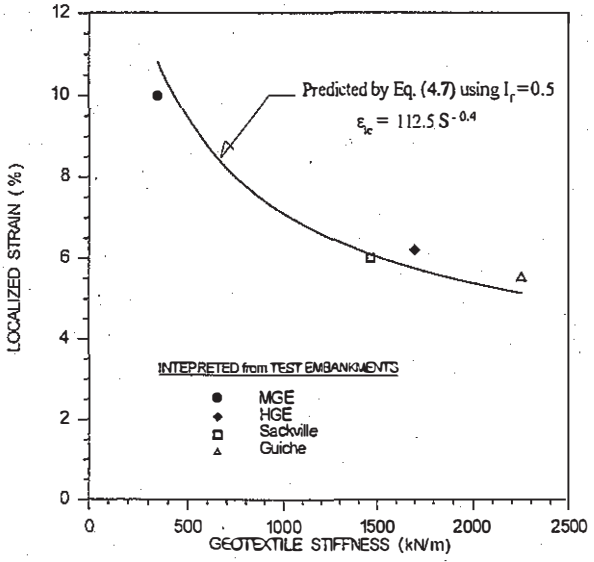

Fig. 13. Interpreted and Predicted Localized Strain in Geotextile Reinforcement.

4 REINFORCED-SOIL STRUCTURE SPANNING PILE FOUNDATIONS OR VOIDS

Three papers were submitted in this category, by Lawson et al, Gartung and Verspohl, and Ohta et al. Based on the measured sagging of embankment base between pile caps and above voids and the reinforcement strain measurements, good

Table 1. Back-Analyses Results for Three Test Embankments Using Actual Properties of Embankment Fill.

Net Embankment Height (m)	FEM Consolidation Analysis	LEM Using Circular Slip Surface								Notes
		Reinforcement				Embankment Fill			FS	
		ε (%)	Tmob (kN/m)	If	Tr (kN/m	γ (kN/m3)	ϕ (deg)	c (kPa)		
CE Embankment										
4.0 m - Case 1						18.5	40	22	1.02	
4.0 m - Case 2	Collapse					18.5	30	15	0.98	
MGE Embankment										
4.2 m - Case 1	Critical	3.0	10.5	0	12.5	19.2	38	17	0.98	
4.2 m - Case 2	Collapse	13.9 *	26.4	0.5	30.5	19.2	30	10	1.00	
HGE Embankment										
4.2 m - Case 1	Critical	2.3	39.1	0		19.2	38	17	1.00	Before induced failure
4.2 m - Case 2		8.5	145	0.5		19.2	30	10	1.25	After induced failure
6.0 m - Case 3	Collapse	13.0	200	0.5		19.2	30	10	1.01	Previous failure surfac
6.0 m - Case 4	Collapse	13	200	0.5		19.2	30	10	1.03	New failure surface

Notes:

1) * Geotextile strain obtained from back calculated value of tensile force for FS = 1
2) All the other values of geotextile strain are taken from the measurements
3) Case 1 and 2 corresponding to strength parameters of embankment fill at peak and critical state, respectively
4) Case 3 using a reduction factor of 0.75 for undrained shear strength of sub-soils along the previous sliding surface

performances of geosynthetic reinforced structure were observed. Furthermore, a unique combination concerning the void space or span, fill height, reinforcement strength, and reinforcement stiffness was obtained to satisfy serviceability criteria. The use of reinforced structure for fills spanning voids or pile is now an increasingly accepted practice.

5 DYNAMIC RESPONSE IN GEOSYNTHETIC REINFORCED STRUCTURES

There were three papers submitted in this category, namely: Fujii et al, Uzuoka et al, and Madabhushi. It was demonstrated that the reinforced embankment maintained its stability under maximum earthquake horizontal accelerations of 310 gals. Moreover, a phase difference was observed between the horizontal inertia force in the reinforced area and the area behind the reinforced zone preventing their simultaneous occurrence. The geotextile reinforcements can control the occurrence of tensile stresses within the reinforced embankment. Increasing the rigidity of the reinforced embankment by increasing the reinforcement stiffness may reduce the amount of deformation and subsidence. Further study is needed to incorporate the results of dynamic response analyses to the seismic design methods of geotextile reinforced embankment. In addition, further studies are needed for the effectiveness of the reinforcement in the prevention of embankment failure and reducing the embankment deformation and subsidence.

6 CONCLUDING REMARKS

The technique of geotextile reinforced embankment has been increasingly used for construction on soft ground foundation. For geotextile reinforced embankment on soft ground,three relevant issues have been dealt with and discussed in this report, namely: the direction of the reinforcing force, the mobilized strains in the geotextile reinforcement, and the modification of soil shear strength at the slip plane. Moreover, a new alternative to geotextile reinforcement, the geosynthetic horizontal drain (GHD), has been developed for utilizing saturated clayey embankment fill. Furthermore, the results of three full scale test embankments with and without geotextile reinforcements constructed to failure are presented in this report. These results confirmed and validated the aforementioned three issues of reinforced embankments on soft ground. Finally, our basic tools to understand and interpret the behavior of reinforced embankment may include theoretical formulation, numerical simulations, full scale tests, laboratory model tests, and design methodology. Considering these tools, the importance of conducting full scale tests together with subsequent data monitoring should be emphasized in order to yield the most valuable and reliable information.

7 REFERENCES

Bergado, D. T., Long, P.V., Lee, C.H. and Werner, G. (1994a), Performance of reinforced embankment of soft Bangkok clay with high strength geotextile reinforcement, Geotextile and Geomembranes, Vol. 13, pp. 403-420.

Bergado, D. T., Long, P.V., Loke, K.H. Christopher, B.R. and Delmas, P. (1994b), Geotextile reinforcement in full scale test embankment on soft ground, Proc. Fifth Int'l. Conf. on Geotextiles, Geomembranes, and Related Products, Singapore, Vol, 1, pp 21-24.

Bergado, D.T., Long, P.V. and Werner, G. (1996), Deformation behavior of geotextile reinforcement at vicinity of shear surface, Proc. First European Geosynthetics Conf. (EuroGeo 1), Maastrict, The Netherlands, pp. 177-182.

Long, P.V., Bergado, D.T. and Balasubramaniam, A.S. (1996), Stability analysis of reinforced and unreinforced embankments on soft ground, Geosynthetics International, Vol. 3, No. 5.

Delmas, P., Queroy,D. Quaresma, M. and De Saint A. (1992), Failure of an experimental embankment: Guiche, Geotextiles, Geomembranes, and Products, den Hoedt (ed), Balkema Printers, Rotterdam, The Netherlands.

Rowe, R. K., Granendran, C. T., Landva, A.O. and Valsangkar, A. J. (1995) Construction and performance of a full scale reinforced test embankment, Sackville, New Brunswick, Canadian Geotech. Journal, Vol. 110, No. 3, pp. 512-534.

Vermeer, P.A. and Brinkgreve R. B. J. (1995), Finite element code for soil and rock analysis, Balkema Printers, Rotterdam, The Netherlands.